Chapter 3

3D Visualization of Microtubules in Epidermal Pavement Cells

Amir J. Bidhendi, Bara Altartouri, and Anja Geitmann

Abstract

The plant cytoskeleton is instrumental in cellular processes such as cell growth, differentiation, and immune response. Microtubules, in particular, play a crucial role in morphogenesis by governing the deposition of plant cell wall polysaccharides and, in consequence, the cell wall mechanics and cell shape. Scrutinizing the microtubule dynamics is therefore integral to understanding the spatiotemporal regulation of cellular activities. In this chapter, we outline steps to acquire 3D images of microtubules in epidermal pavement cells of *Arabidopsis thaliana* cotyledons using a confocal microscope. We introduce the steps to assess the microtubule distribution and organization using image processing software Bitplane Imaris and ImageJ. We also demonstrate how the interpretation of image material can be facilitated by post-processing with general-purpose image enhancement software using methods trained by artificial intelligence-based algorithms.

Key words Cytoskeleton, Microtubules, Pavement cells, Confocal microscopy, 3D analysis, MAP4, Propidium iodide, Bitplane Imaris, ImageJ, Artificial intelligence, Image enhancement, Topaz Labs

1 Introduction

The plant cytoskeleton is involved in a host of cellular activities including sensing and responding to intrinsic and extrinsic cues such as pathogen attack and wound response, cell wall deposition, cell growth, and differentiation [1]. These processes underlie feedback loops that operate at tissue, cell, and subcellular scales. Microtubules are a key element of many of these feedback loops through their involvement in both sensing and response [2–4]. A key response is mediated by the microtubules' influence on cellulose deposition by way of marking the location of the insertion of cellulose synthase complexes into the plasma membrane and guiding the movement of the enzymes [1, 5]. Microtubules thus influence cell wall mechanical anisotropy and exert spatiotemporal control on cell growth [2, 6, 7]. Our understanding of the involvement of the cytoskeleton in complex developmental signaling and

Patrick J. Hussey and Pengwei Wang (eds.), *The Plant Cytoskeleton: Methods and Protocols*,
Methods in Molecular Biology, vol. 2604, https://doi.org/10.1007/978-1-0716-2867-6_3,

response mechanisms in plants is expanding, but it remains limited by our ability to monitor related processes in real time and in 3D. A deeper understanding necessitates improved tools combining high-resolution microscopical techniques and live probes with complementary experimental approaches such as mechanical testing [8–10].

Epidermal pavement cells at the leaf surface of many plant species form intriguing shapes that resemble interlocking pieces of a jigsaw puzzle. The generation of these shapes has been shown to involve intricate coordination of events implicating the cortical microtubules linking mechanical instability, cell geometry, mechanical stress, and cell wall chemistry [2, 11, 12]. In this chapter, we provide a step-by-step protocol to visualize and quantify the pavement cell microtubules in 3D.

2 Materials

2.1 Plant and Plant Growth Material

1. *Arabidopsis* fluorescent marker line for microtubules, e.g., GFP-MAP4 [13].
2. 100% ethanol (EtOH).
3. Double-distilled autoclaved water (ddH_2O).
4. Bleach.
5. Murashige and Skoog (MS) salt mixture.
6. Sucrose.
7. 1N KOH.
8. Agar.
9. Eppendorf tubes.
10. Pipette tips.
11. Glass bottle.
12. Petri plates.
13. Parafilm.

2.2 Fluorescence Labeling and Sample Mounting

1. Propidium iodide (PI).
2. Tweezers.
3. Microscope slides.
4. Coverslips.
5. Kimwipe paper.

2.3 Microscopy and Image Processing

1. Confocal laser scanning microscope or spinning disk microscope with high numerical aperture (NA) objective.
2. ImageJ or Fiji software or equivalent image processing software.

3. Bitplane Imaris software or equivalent image analysis software.
4. Artificial intelligence (AI)-based image enhancement software, e.g., Topaz Labs' Gigapixel AI (optional).

3 Methods

3.1 Seed Sterilization and Stratification

For demonstration purposes in this chapter, we use *Arabidopsis thaliana* because of the large inventory of fluorescent protein-expressing lines (RFP, GFP, and YFP) for this species. In choosing the optimal fluorescent protein marker line for the experiment, one must carefully consider imaging parameters (*see* **Notes 1–3**).

There are several methods for seed sterilization and stratification that can be suitable for different usage scenarios. The protocol presented here is time-efficient, and it is most suitable when seeds are to be used for sowing within a few days to 1–2 weeks after sterilization. The method is based on ethanol and bleach and was observed to yield a high rate of seed germination as well as a low rate of seed mortality and contamination pre- and post-germination.

1. Work in sterile conditions with autoclaved and sterile tools inside a laminar flow hood.
2. Transfer the required amount of *Arabidopsis* seeds to an Eppendorf tube, filling only the very bottom (e.g., 2–3 mm) to allow room for proper sterilization and rinsing in the next steps. If necessary, use multiple tubes.
3. Fill the tube with 100% ethanol (EtOH). For 15 s, gently agitate the tube to maximize flow and contact between the ethanol and seed surfaces.
4. Promptly remove the EtOH using sterilized pipette tips.
5. Fill the Eppendorf tube with double-distilled autoclaved water (ddH_2O). Keep agitating the tube for 20 s.
6. Remove the ddH_2O using sterilized pipette tips, and cover the seeds with 50% commercial bleach. Gently agitate the tube for 5 min. This can be performed either manually or using a tube rotator. Ensure that seeds do not make aggregates so that the bleach solution can efficiently reach the seed surfaces.
7. Remove the bleach and rinse the seeds three to five times by filling the Eppendorf tube with autoclaved ddH_2O, gently shaking the tube each time for 20 s before replacing the ddH_2O with fresh liquid.
8. Leave the seeds in the tube half-filled with autoclaved ddH_2O. Wrap the Eppendorf tubes in aluminum foil, and leave them in the fridge in the dark at 4°C for 3–4 days for stratification. After this period, seeds can be used for seeding (*see* **Note 4**).

3.2 Preparation of ½ MS Growth Medium

1. Pour 900 mL of ddH_2O into a beaker, and add 2.2 g MS salt mixture [14]. Once the salt is dissolved, adjust the pH to 5.6–5.8 using 1N KOH.
2. Add 10 g sucrose.
3. Adjust the volume of the solution to 1 L with ddH_2O.
4. Pour media into a glass bottle suitable for autoclaving.
5. Add 8 g plant agar, and gently stir the solution (agar will remain granular since it does not dissolve at room temperature).
6. Autoclave using the appropriate program for liquids.
7. Let the solution cool to a moderately warm temperature. This can be achieved slowly by leaving it under the hood or more rapidly by bathing the bottles in cold water in the sink. Do not let the solution become too cold as the medium will begin to solidify complicating pouring and distribution into Petri plates.
8. Pour the solution into sterilized Petri plates, and let the media solidify under the hood (*see* **Note 5**).
9. The plates can be stored for up to a month in the fridge at 4 °C.

3.3 Seed Germination and Growth

1. Working in sterile conditions under the hood, remove the seeds from the Eppendorf tubes, for example, by using autoclaved pipette tips, and place them on the surface of the solid MS medium (*see* **Note 6**).
2. Seal the plate lids using Micropore tape or Parafilm strips, and place them in the growth room under appropriate lighting conditions (e.g., 16-h-long lighting).
3. Check the samples sporadically for growth and/or contaminations. Collect the seedlings at a proper stage (e.g., 2 days) after germination for mounting and microscopical observation (*see* **Note 7**).

3.4 Preparation of Secondary Fluorescent Labeling Solution

To visualize the borders of pavement cells, here we use propidium iodide (PI) in parallel to the natively expressed GFP. PI binds cell wall polysaccharides, is easy to work with, and is compatible with live imaging [9, 11] (*see* **Notes 8** and **9**).

1. Dissolve the PI, if obtained in powder form, at the desired concentration in ddH_2O in an Eppendorf tube. A concentration of 0.5–1 mg/ml was observed to produce a bright signal in pavement cell walls. Vortex the tube. For time-lapse studies, using considerably lower concentrations (e.g., 0.01 mg/ml) might be beneficial to minimize toxicity, stress, or altered growth (*see* **Note 10**).
2. PI stock solutions can be prepared and stored in aliquots. Keep the stock in the dark in the fridge (4°C). For longer-term storage, we did not observe any degradation in the quality of the stain resulting from freezing and thawing.

3.5 Secondary Fluorescent Labeling of Arabidopsis Seedlings

1. Using tweezers, remove the seedlings from the Petri plates, and place them on a glass slide or an empty Petri plate. Care must be taken to place the tweezer tips beneath the cotyledons to gently lift the seedlings rather than squeezing them.
2. Cover each seedling with one to two drops of the PI staining solution. Ensure that the seedling is fully immersed in the staining solution. Cover the samples to protect them from light.
3. After 5–10 min, remove the PI solution using a pipette or a piece of Kimwipe paper, and rinse the seedlings three times using ddH_2O. Rinsing can be performed by placing a few drops of ddH_2O on each seedling for 15–20 s before removing and replacing the liquid with fresh rinsing solution. The seedlings are now ready to be mounted for microscopy.

3.6 Mounting Samples on Slides for Microscopical Observation

1. Gently place each seedling on one to two drops of ddH_2O on a glass slide (*see* **Note 11**). Place one edge of a coverslip on the water, and slowly lower the other edge so that the cotyledons are gently flattened between the slide and the coverslip for a proper field of view and ease of focus during microscopy. If the seedlings are too large, the thickened stems can prevent a good seal or proper imaging of the cotyledons. Spacers can be used to adjust the distance between coverslip and slide (*see* **Note 7**).
2. Gently press on the edges of the coverslip using a piece of Kimwipe paper to squeeze out and absorb excess mounting liquid, if any, from below the coverslip. This will allow a better seal and focus and prevent displacements of the coverslip during imaging.
3. Perform the imaging as soon as possible. Keep the samples in dark conditions before and during imaging (*see* **Note 12**).

3.7 Confocal Microscopy for Imaging Microtubules in Epidermal Pavement Cells

We use a Zeiss LSM 510 META confocal microscope at basic settings for imaging in the present chapter (*see* **Note 13**). Other confocal microscopes provide similar functionality under similar settings.

1. Locate the region of interest on the cotyledon in brightfield mode at low light intensity settings.
2. Switch to the laser scanning mode by choosing the appropriate settings including the laser, excitation, and emission filters.
3. We used excitation wavelengths of 532 nm and 489 nm and emission windows of 590–625 nm and 500–530 nm for PI and GFP channels, respectively.
4. Choose an objective with proper magnification based on the region of interest and detail to be studied. For a given magnification, choose the objective that has the highest NA for the best results.

5. Adjust the laser power to an acceptable minimum to avoid photobleaching or stressing the samples. Determine an optimal combination set of scanning parameters, including laser power, digital gain, pinhole diameter, scanning speed, and image size (*see* **Notes 13–15**).
6. After determining the optimal scanning parameters, the scanning depth must be determined. This is performed by setting the first and last slices of the z-stack and determining either the number of slices or the distance between slices. Generally, the microscope software allows choosing optimal z-step distance based on the used objective and the pinhole diameter (*see* **Notes 16** and **17**).
7. Choose the beginning and end levels of the z-stack to start the scanning well above the sample surface and end below the target structure. Note that the periclinal walls of pavement cells bulge outward and hence form highly curved surfaces. To fully capture the outer half of the epidermal cell layer, the starting z-level should therefore be above the highest bulge, and the lowest z-level should capture the anticlinal walls of all cells in the field of view without leaving any gaps. If in doubt, it is generally preferable to acquire more than less (*see* **Note 18**).
8. Save the z-stacks in proper format with all relevant experimental notes (e.g., time and date, treatments, etc.; *see* **Note 19**).

3.8 2D Image Analysis by Projecting the 3D Data on a Plane

Analyses of micrographs and z-stacks can be performed in 2D or 3D depending on the level of detail required and the type of information desired. 2D analysis of the z-stacks is the first stage in the image analysis routine because it requires fewer computational resources and can easily be performed using freely available platforms such as ImageJ (https://imagej.nih.gov/ij/) or Fiji (https://imagej.net/software/fiji/). Here we provide a step-by-step procedure to obtain information on the distribution of microtubules along the wavy borders of pavement cells. For this demonstration, we rely on z-stacks acquired from the GFP channel only. The process for merging a second channel into the final projection is very similar to the one described below for adding a single optical section. The use of a second channel will be discussed in the next sections (3D visualization).

1. Launch the ImageJ (or Fiji) program, and open the corresponding micrograph (here in .lsm or .czi format). To open the file format, sometimes additional ImageJ plugins such as Bio-Formats are necessary which can be added to the ImageJ plugin library, if not already included.
2. Scroll down in the z-stack until the slice in which the anticlinal borders of all or most cells within the region of interest are visible (Fig. 1a). For this, flat cotyledons are particularly helpful at high magnification because curved organ surfaces lead to the

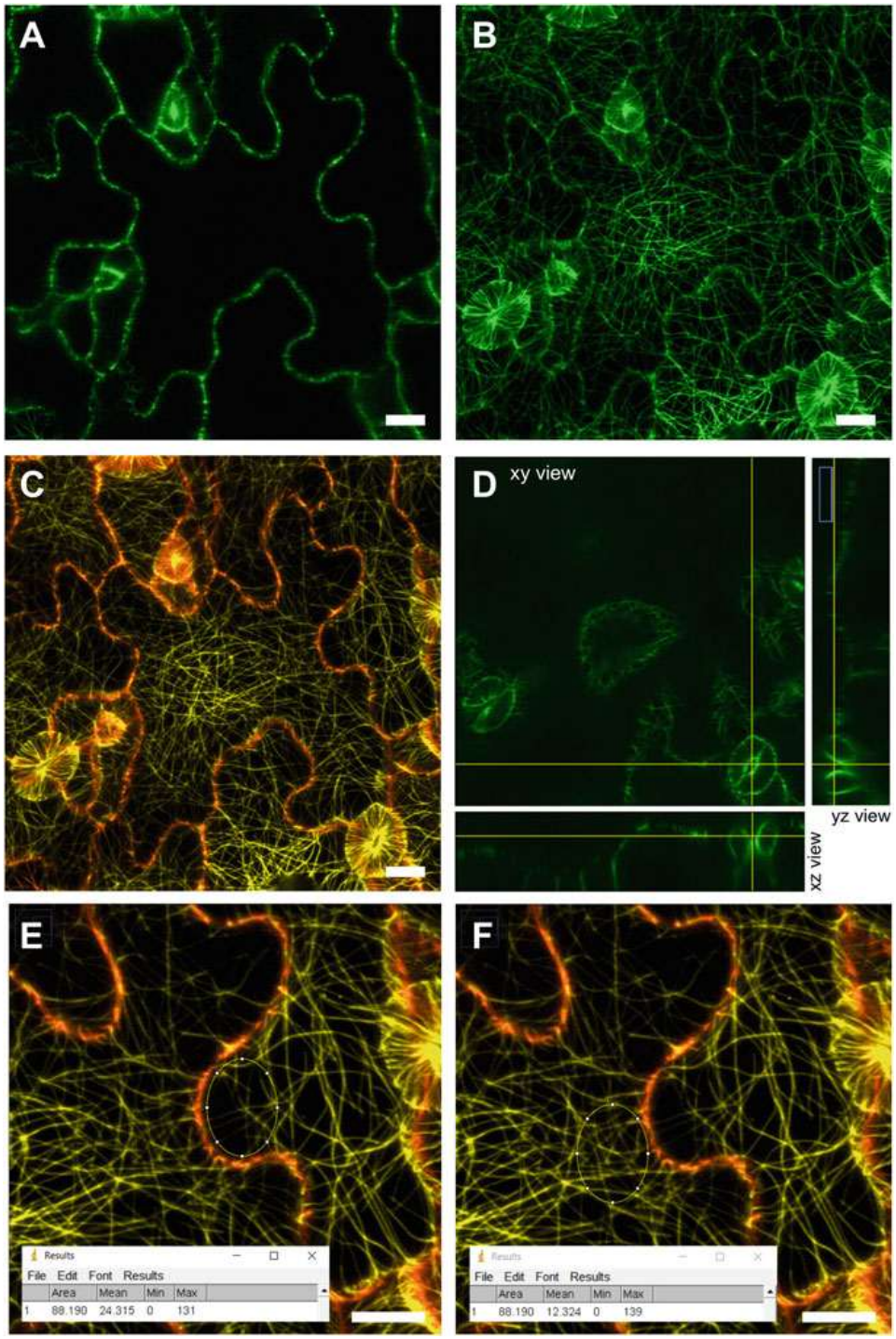

Fig. 1 2D analysis of confocal microscope z-stack of microtubules in GFP-MAP4 pavement cells. (**a**) A single optical slice showing epidermal cells of *Arabidopsis* GFP-MAP4 cotyledon. A slice to capture most of the cell borders is generally located at the mid-depth of the epidermal layer and can be duplicated, pseudo-colored, and used to mark cell borders in z-projections of the 3D stack. (**b**) Maximum intensity z-projection of the confocal microscope z-stack showing microtubules of epidermal pavement cells in 2D. (**c**) The slice in (**a**) is merged into (**b**) to mark cell borders using a different pseudo-color (red, single slice as in (**a**); yellow, same stack as in (**b**). (**d**) Orthogonal views are useful to assess structures oriented perpendicular to the xy plane. Yellow lines in xy view indicate the locations of the orthogonal yz and xz views. (**e** and **f**) ROIs can be determined using Selection tools (here oval). Microtubule density can be evaluated using Analyze → Measure. Here the value for "mean" is the mean pixel signal intensity in each oval ROI and indicates that the signal (and hence the microtubule density) is higher adjacent to the indentation side of a cell border undulation (mean = 24.3) compared to the opposing protrusion side (mean = 12.3). Scale bars = 10 μm

border of some cells falling out of the focal plane requiring increasingly deeper scans. Duplicate the selected optical slice (Shift+D in windows or using the Image drop-down menu). Uncheck "duplicate stack."

3. If needed, the contrast and brightness of the selected slice can be adjusted (Shift+C or from the Image drop-down menu → Adjust). You can leave this micrograph open or save it (.tiff).
4. To analyze the microtubule distribution in 2D, a z-projection can be performed. z-Projection can be performed using Image → Stacks → Z Project (Fig. 1b). Enter the number of first and last z-slices of interest. Choose the desired type of projection depending on the type of analysis, or if unsure start with max intensity. Duplicate the resulting projection to generate a separate working file for the next steps.
5. A slice from a different channel such as the one used for the PI signal can be merged into a composite micrograph to outline cell borders in microtubule-dense regions.
6. Alternatively, to facilitate distinguishing the pavement cell borders using microtubule data only, a composite figure can be produced with the pseudo-colored border slice obtained previously (Fig. 1a) merged into the result of the z-projection (Fig. 1b). For this, with both border and z-projected micrographs open in ImageJ, use Image → Color → Merge Channels. Choose the desired color channels for each item from the drop-down menus. Check "Create composite," "Keep source images," and "Ignore source LUTs" (Fig. 1c). Before this, images can be set at suitable types and bit depths (Image → Type → RGB, 16-bit, or 32-bit). The resulting micrograph can be saved in desirable type and format (e.g., RGB, .tiff).
7. Measurements such as average signal intensity can be performed within a region of interest (ROI) using Area Selection tools and Analyze → Measure (or M). Before this, set the desired parameters that are to be included in the report. For this, go to Analyze → Set Measurements. For example, here we checked "Area, Mean gray value, Standard deviation, Min & Max gray value, and Display label." To perform repeated measurements and comparisons, such as comparing the microtubule density on two sides of a border undulation, the selected ROI marker can be moved to different locations on the image using the cursor (Fig. 1e, f).
8. To detect structures oriented in the z-direction, orthogonal projections can be performed in x or y directions similarly to z-projection. Orthogonal views (Image → Stacks → Orthogonal views) can also be very helpful as they allow observing the same region from different views (Fig. 1d).

9. If a substantial and non-uniform background signal is present, the estimation of microtubule density based on signal intensity within a selected ROI may be less reliable. Moreover, this approach does not provide information on the directionality of microtubules and does not consider the microtubules aligned perpendicular to the plane of view. To analyze the distribution and orientation of the fibril-like structures, tools such as the FibrilTool can be used [15]. Microtubule orientation can be analyzed on 2D projections yielding useful information on the cortical microtubules along the periclinal or anticlinal walls, respectively. However, 2D projections do not allow for the assessment of microtubules that change orientation in space, e.g., when curving at a cell edge. To obtain full details on the spatial distribution of the cytoskeleton, 3D analysis may be the only option. While ImageJ allows for some level of 3D reconstruction and analysis (e.g., Image → Stacks → 3D Projection), here we will demonstrate the use of an alternative powerful image analysis tool, Bitplane Imaris.

3.9 3D Image Analysis on the Spatial Distribution of Microtubules

Cellular structures are inherently 3D objects. While 2D analysis techniques in many cases provide valuable insight, they can also obscure crucial 3D details. Bitplane Imaris is a powerful commercial software for 3D and 4D analysis of microscopical images. Both the free and full versions of the Imaris software offer attractive functionalities for visualization of confocal z-stacks. In this section, we use the full version Imaris 9.8 (https://imaris.oxinst.com) to visualize z-stacks obtained from GFP and PI channels. Steps to import the stacks are as follows.

1. Imaris "Arena" is the starting point for importing the z-stacks and converting files to Imaris file format (Fig. 2a). This module allows managing folders and files. Image files and stacks can be processed individually or in batch mode (e.g., File → Batch convert). Under "Arena," use "Observe Folder" to add a folder path containing the z-stacks. Right-click on the z-stacks, and select "Convert to native Imaris file format" to convert them to .ims format (Fig. 2b).
2. In the "Surpass" view, open the z-stack by File → Open, and locate the .ims file of the converted z-stack. The z-stack can be viewed in either 3D or slice view. In slice view, the slice number can be adjusted using the slider (Fig. 2c). Image brightness and contrast can be adjusted in the Display Adjustment toolbar via setting the min. and max. values in the histogram (*see* **Note 20**). The pseudo-color assigned to the channel can be adjusted by clicking on the channel number (e.g., chL1) in Display adjustment (Fig. 2c–7).

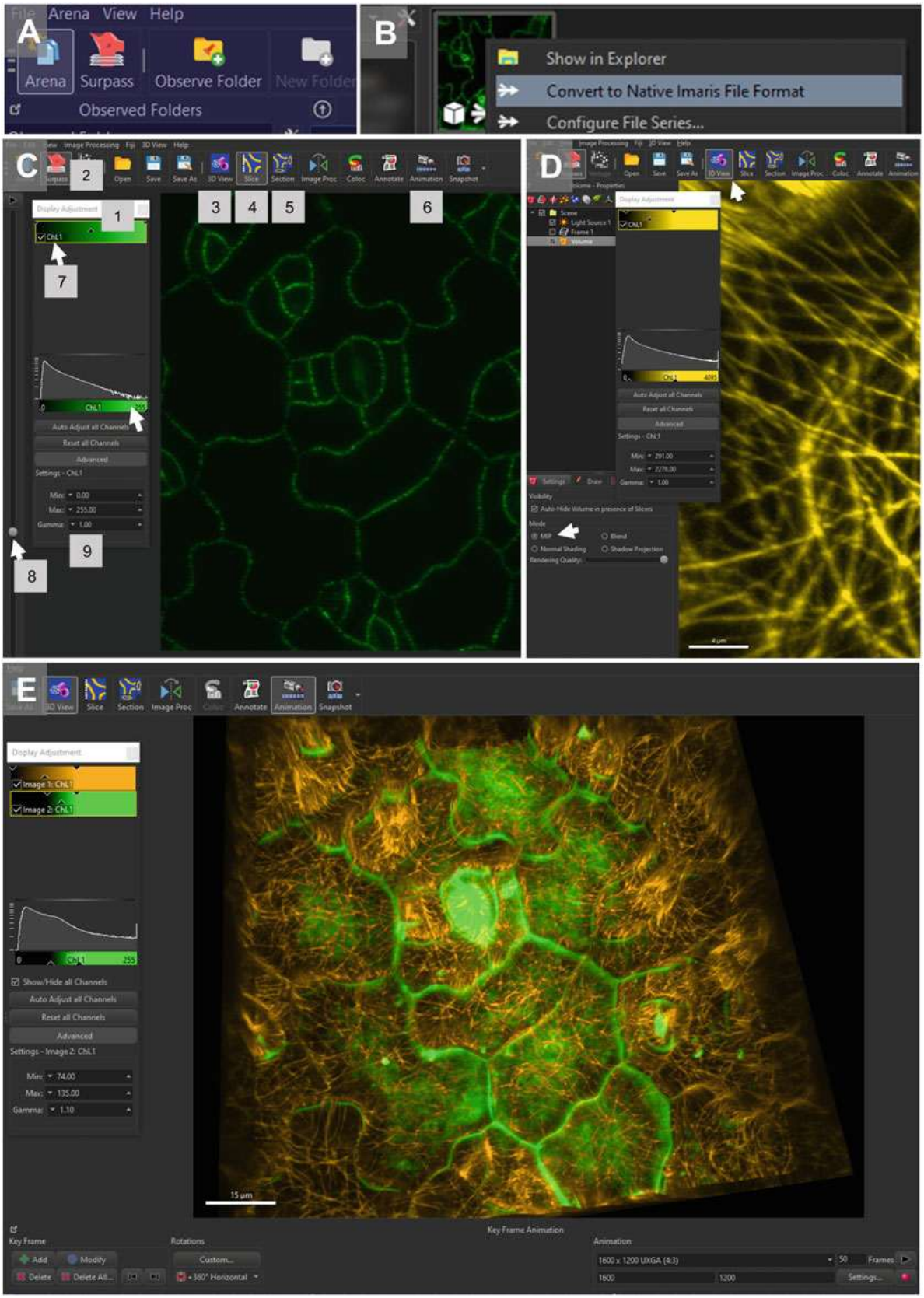

Fig. 2 Imaris software used for 3D visualization of confocal z-stacks of microtubules in pavement cells of the *Arabidopsis* GFP-MAP4 line. (**a**) Arena is the environment used for file management and conversion. (**b**) Input stack or images or image series are converted to native Imaris format (.ims) in Arena environment. (**c**) Some

3. In 3D view mode, the basic MIP (maximum intensity projection) can be used to visualize the z-stack. The resulting 3D object can be translated and rotated using right and left mouse buttons. The scroll wheel can be used to zoom in and out of a region (Fig. 2d).
4. To visualize the cell borders using the z-stacks from the PI channel, additional images can be imported and added to the existing volume. This can be achieved by File → Add image and choosing the .ims file corresponding to the z-stack of interest. In the same fashion as with the previous channel, the intensity level of the second channel can be adjusted to allow revealing the appropriate level of details between the two overlapping stacks (Fig. 2e).
5. For presentation and publication purposes, animations can be made using the Animation tool in the Surpass environment. Animation can be created by adding "Key Frames" entailing two or several translations and rotations to create a desirable camera path and perspectives based on features of interest. The resulting animation can be played back, recorded, and saved under the options for the Animation tool (Fig. 2e).

3.10 Potential for Artificial Intelligence-Based Post-Acquisition Image Enhancement in the Interpretation of the Subcellular Organization of Microtubules

It is crucial to aim for the best-quality images at the sample preparation and image acquisition steps to eliminate the need for excessive image post-processing (*see* **Note 21**). Here we introduce sample images of microtubules in pavement cells processed using Topaz Labs' Gigapixel AI (v5.8)—a photo enlargement software that uses trained AI model to enlarge, deblur, and denoise photos (https://topazlabs.com/gigapixel-ai).

1. Save the z-stack as individual .tiff images using ImageJ, File → Save as → Image sequence → .tiff.
2. Import the Image sequence in Topaz Lab's Gigapixel AI by File → Open images (select all).
3. In the imported images, select a slice that includes regions with in-plane microtubules. This slice will be used to adjust enhancement parameters for the whole batch.

Fig. 2 (continued) Surpass environment tools and options used to configure and visualize the images and 3D stacks: Display Adjustment module (1), Surpass environment button (2), 3D view (3), Slice view (4), Section or orthogonal views (5), Animation tool (6), Channel pseudo-color adjustment (7), Slice selection slider (8), and Histogram parameters (9). A single slice of a z-stack is shown in the figure. (**d**) MIP display mode is used to visualize the z-stack in 3D using the 3D view option. (**e**) A separate z-stack (propidium iodide channel, green) is added to the existing GFP-MAP4 stack (orange) to mark the cell borders. Channel histograms can be adjusted individually in the Display adjustment module. Using the Animation tool, animations can be produced by adding Key frames at various locations and angles guiding the relative trajectory of the camera and the 3D stack

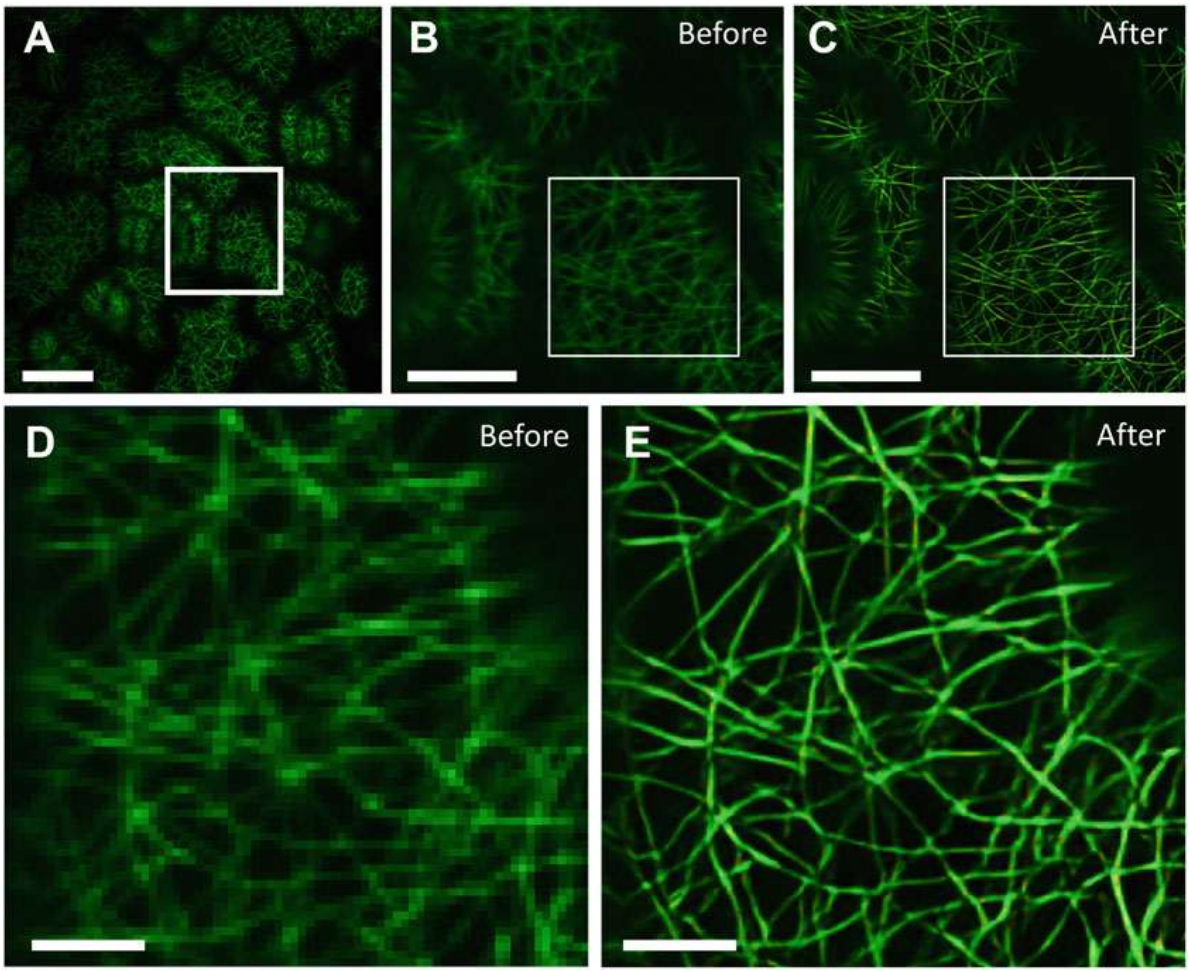

Fig. 3 A single optical section of a z-stack of *Arabidopsis* MAP4 GFP marker line used for AI-based image enhancement using Topaz Lab's Gigapixel AI. (**a**) Confocal micrograph of microtubules marked with GFP-MAP4. (**b** and **d**) Different magnification levels of the micrograph in (**a**) before AI-based enhancement. (**c** and **e**) Areas in (**b**, **d**) after AI-based enhancement. Apparent uneven abundance of microtubules across the field of view in (a, b, c) result from outward bulging of cells. The single optical slice shown captures only the most elevated areas of the bulges. Scale bars = 20 μm (**a**), 10 μm (**b**, **c**), and 3 μm (**d**, **e**)

4. From the viewfinder, select and zoom in a suitable region (Fig. 3a).
5. Choose the scaling factor or set the desired width and height of the image for image enlargement. Select the AI model that produces the best result through trial and error adjusting the method parameters. This can be performed using the side-by-side view to compare the original image (Fig. 3b, d) with the updated result (Fig. 3c, e).
6. The determined settings are automatically applied to all selected images. Use "Save all" to batch process and export the image series.

7. To use the processed images for 3D visualization, the image series exported from Gigapixel AI can be imported into Imaris. To this end, in Imaris, add the folder containing the images to the "observed folder" path as described before.
8. Right-click on the thumbnail of the image appearing in the folder in Arena, and choose "Configure file series." Adjust the series parameters, particularly the z-step, which can be obtained from the metadata of the original stack.
9. Convert the series by right-clicking on the thumbnail and choosing "Convert to Imaris Native File Format." The enhanced 3D stack can now be visualized in Surpass environment as described previously (*see* **Notes 22–24**).

4 Notes

1. To choose the optimal fluorescent protein line for an experiment, one must consider several parameters including but not limited to:
   - Emission and excitation wavelengths to avoid or at least minimize spectral overlap with those of other fluorescent probes such as dyes used for labeling cell wall polysaccharides.
   - Brightness and photostability (resistance to photobleaching) of a given fluorescent protein.
   - Likelihood of the fluorescent protein oligomerization as well as potential changes in the functioning of the attached protein.
2. For live-cell imaging of cortical microtubules, the commonly used lines involve microtubule-binding protein markers such as MAP4 and MAP65 and tubulin markers such as TUA5, TUA6, and TUB6.
3. Seeds and plants of any mutant line must be discarded according to corresponding protocols and regulations such as by autoclaving them before disposal.
4. The presented method for seed sterilization and stratification eliminates the need for additional steps such as seed dehydration after sterilization and works best if the seeds are to be used within a short period (e.g., 1 week). Keeping the seeds in the fridge substantially longer may affect their viability, germination, and growth rate.
5. To avoid condensation and droplets forming on the inside of the lid or on the media, which can promote microbial growth, leave the plate lids partly open.

6. Allow sufficient spacing between the seeds (e.g., 5 mm from each side) to prevent the entangling of seedling radicles as they grow and facilitate their harvesting in the next steps. Avoid transfer of excess liquid with the seeds from the Eppendorf tubes.
7. Seedlings typically germinate between 48 and 72 h after sowing. For visualization of microtubules using GFP lines, cotyledons of seedlings between 2 and 5 days after germination were found to be most amenable to study. At later stages, the cotyledons grow too large and form curved surfaces preventing proper mounting (if mounted on microscope slides with coverslips). On the other hand, visualizing microtubules of the epidermal layer of the cotyledon at the early stages (e.g., 1–2 days after germination) will allow approaching the abaxial side of the cotyledon very close to the coverslip because the cotyledons are closed. If the cotyledons are studied at later stages, particularly for time-lapse studies, we recommend the use of double-sided tape as a spacer. Beneath the cotyledon, place either a thin layer of solid MS media or a tape to minimize the distance between the cotyledon and the coverslip. In this case, the abaxial or the adaxial sides of the cotyledon can be visualized while minimizing the compressive forces from the coverslip (*see* also **Note 11**).
8. A second probe can be used to illuminate the cell borders. This can be achieved using fluorescent probes with affinity to either the plasma membrane or cell wall polysaccharides. If a dye is chosen, it should be suitable for live-cell imaging: it must be easy to apply to the samples and should not interfere with cell growth over the course of time-lapse experiments. A common plasma membrane stain is the lipophilic dye FM4-64. Some of the common cell wall dyes are PI, Pontamine fast scarlet 4B (S4B), and calcofluor white [9]. Calcofluor white is a fluorescent blue dye, whereas PI and S4B are fluorescent red dyes. Calcofluor white and S4B label cellulose with different affinities, while PI binds the negatively charged pectin in the wall. All these probes have been successfully used for live-cell imaging [9, 11, 16]. PI was particularly useful in the case of pavement cells because its application is easy, it readily penetrates the cuticular layer—at least in cotyledons—and it does not interfere with cell growth at moderate concentrations.
9. Always consult the material safety data sheets (MSDS) for any new material used in experiments. PI is a known mutagen and must be handled with care. The liquid and solid waste including the rinsing solutions as well as tools and containers must be discarded and cleaned according to safety and hazardous waste regulations.

10. The cytoskeleton is highly dynamic with high rates of polymer growth and depolymerization. Therefore, snapshot images of cytoskeletal configuration must be interpreted accordingly, and, in some cases, time-lapse imaging may provide better insight than single snapshots.
11. Microtubules are known to respond to changes in mechanical stress. Indeed, pressing the seedlings between coverslip and glass slide can lead to altered microtubule dynamics and organization [17]. While at the subcellular scales, the mechanical stresses are presumably sufficiently large to overcome contact pressure-induced microtubule reorientation, the tissue-level organization of the cytoskeleton might still be affected to some degree and at least transiently. Therefore, using immersion objectives eliminating the need for coverslips is highly preferred.
12. The procedure listed in this chapter is tailored to one-time observations of the seedlings using a non-immersion microscope objective. If long-term time-lapse experiments are intended, seedlings must be handled extremely gently to avoid mechanical damage, ensuring that radicles are in contact with medium at all times and that sample transfer to and from growth chambers between imaging sessions is swift. For this purpose, microscope mountable growth slides can be invaluable [9, 11].
13. Laser scanning confocal microscopes produce high-quality low-noise z-stacks. However, the exposure times in this imaging modality can sometimes be too long for time-lapse experiments leading to photobleaching of the fluorescent proteins or phototoxicity. These issues can be reduced by using a spinning disk confocal microscope.
14. The optimal percent of the laser power will depend on various parameters such as the quality of labeling, wavelength, scanning speed, as well as total power output of the laser.
15. Ideally, the acquired images are obtained at maximum resolution (in terms of the number of pixels) with a pinhole set as close as possible to one Airy unit diameter to minimize out of focus light. However, in practice, compromises need to be made to obtain z-stacks at reasonable speed to minimize sample damage. The scanning parameters will largely depend on factors such as the type of fluorophore, the quality of labeling, as well as the depth of the sample to be scanned.
16. Undersampling—using a slice distance larger than optimal—can lead to spatial aliasing reducing the usefulness of micrographs, particularly for publication purposes. Undersampling can be helpful to gain speed when image quality is not a concern, especially during the initial phase of trial and error and parameter optimization. Oversampling, on the other hand,

can produce high-quality images but at the expense of the risk of photobleaching. This can lead to non-uniform signal intensity through the depth of the z-stack as the sample is getting increasingly bleached.

17. Sample drift in the 3D and temporal dimensions, e.g., due to the movement of the sample during the acquisition or due to plant growth, can represent an experimental challenge. If the drift occurring during a single z-stack and acquisition cannot be mitigated by modifying the mounting method, we recommend a faster acquisition time. For a time-lapse experiment, sample drift may occur in xy and z-directions. We recommend using a larger scanning area and larger upper and lower limits so that there are at least three z-steps above and below the top and bottom surfaces of the sample or the target structure, respectively. If drift occurs during the study, it may be corrected during post-processing using tools such as the 4D drift correction plugin in ImageJ [18].
18. Insufficient scanning range can render the data useless or even misleading. Unfortunately, gaps between neighboring cells resulting from an insufficient depth of the z-scan have sometimes been mistakenly referred to as the middle lamella—the adhesive layer between plant cells. Choosing a z-level that captures the inner periclinal walls and adjacent mesophyll, therefore, ensures that such errors in interpretation are avoided and that abundant information for post-acquisition analysis is generated.
19. Confocal micrographs are generally saved automatically with their metadata. Metadata contain information such as the objective used, wavelengths, and pinhole diameter. The file formats vary between microscope brands and models. For Zeiss microscopes, z-stacks are generally stored as .lsm or .czi formats that can be viewed using open-source or proprietary software such as Zeiss Zen, Imaris, or ImageJ.
20. Nonlinear adjustments such as gamma correction must be reported along with the results. Adjustments such as brightness and contrast must be performed identically for the control and other conditions, certainly if fluorescence intensity is to be compared.
21. In some situations, judicious application of post-processing routines can aid in interpreting the data, however. Suboptimal image quality may be inevitable, for example, when higher scanning speeds are required to minimize photobleaching, when samples are poorly mounted, or when signal intensity decreases with increasing scanning depth. The resulting loss of image quality renders the recognition of spatial localization and distribution of microtubules challenging. Recent years have seen a growing number of tools developed to automate feature

detection from microscopy images. FibrilTool [15] and SOAX [19] are examples of toolboxes that enable automated and reproducible detection and quantification of fibrillar structures such as microtubules which can benefit from improved image quality. AI-based packages specially trained for handling microscopical images, such as NIS.ai by Nikon, TruAI by Olympus, and ZEN Intellesis by Zeiss, show a great potential in establishing trainable image segmentation and enhancement pipelines for tasks such as deblurring, denoising, removing out of focus light, and feature recognition. Interestingly, we observed that even some of the general-purpose AI-based image enhancement packages not specifically trained to handle microscopical images can produce stunning results.

22. These image manipulation procedures can easily introduce false information, e.g., non-existing microtubule branches. The enhancement parameters and results must be scrutinized and considered in this context.
23. Studies are warranted to evaluate the efficacy and accuracy of image enhancement using such tools. We performed some tests by adding simple noise and blur effects to original images followed by rescuing the images using Gigapixel AI. While the results were stunning (not shown), an in-depth study of noise and blur relevant to microscopy experiments must be performed.
24. Ultimately, as with any image manipulation, these image modifications should be approached with utmost caution and disclosed when submitted for publication.

Acknowledgments

This study was supported by a Discovery Grant from the Natural Sciences and Engineering Research Council of Canada (NSERC) to A.G. and by the Canada Research Chairs Program. Image acquisition was performed at the McGill University Multi-Scale Imaging Facility, Sainte-Anne-de-Bellevue, Québec, Canada.

References

1. Chebli Y, Bidhendi AJ, Kapoor K, Geitmann A (2021) Cytoskeletal regulation of primary plant cell wall assembly. Curr Biol 31:R681–R695
2. Bidhendi AJ, Altartouri B, Gosselin FP, Geitmann A (2019) Mechanical stress initiates and sustains the morphogenesis of wavy leaf epidermal cells. Cell Rep 28:1237–1250.e6
3. Landrein B, Hamant O (2013) How mechanical stress controls microtubule behavior and morphogenesis in plants: history, experiments and revisited theories. Plant J 75:324–338
4. Sampathkumar A, Krupinski P, Wightman R, Milani P, Berquand A, Boudaoud A, Hamant O, Jönsson H, Meyerowitz EM (2014) Subcellular and supracellular mechanical stress prescribes cytoskeleton behavior in

Arabidopsis cotyledon pavement cells. Elife 3: e01967

5. Chan J, Coen E (2020) Interaction between autonomous and microtubule guidance systems controls cellulose synthase trajectories. Curr Biol 30:941–947.e2
6. Bidhendi AJ, Geitmann A (2016) Relating the mechanics of the primary plant cell wall to morphogenesis. J Exp Bot 67:449–461
7. Cosgrove, Daniel J (2022) Building an extensible cell wall. Plant Physiology 189:1246–1277
8. Bidhendi AJ, Geitmann A (2018) Tensile testing of primary plant cells and tissues. In: Geitmann A, Gril J (eds) Plant Biomechanics: From Structure to Function at Multiple Scales. Springer International Publishing, Cham, pp 321–347
9. Bidhendi AJ, Chebli Y, Geitmann A (2020) Fluorescence visualization of cellulose and pectin in the primary plant cell wall. J Microsc 278: 164–181
10. Robinson S, Durand-Smet P (2020) Combining tensile testing and microscopy to address a diverse range of questions. J Microsc 278:145–153
11. Altartouri B, Bidhendi AJ, Tani T, Suzuki J, Conrad C, Chebli Y, Liu N, Karunakaran C, Scarcelli G, Geitmann A (2019) Pectin chemistry and cellulose crystallinity govern pavement cell morphogenesis in a multi-step mechanism. Plant Physiol 181:127–141
12. Bidhendi AJ, Geitmann A (2019) Geometrical details matter for mechanical modeling of cell morphogenesis. Dev Cell 50:117–125.e2
13. Marc J, Granger C, Brincat J, Fisher D, Kao T, McCubbin A, Cyr R (1998) A GFP-MAP4 reporter gene for visualizing cortical microtubule rearrangements in living epidermal cells. Plant Cell 10:1927–1940
14. Murashige T, Skoog F (1962) A revised medium for rapid growth and bio assays with tobacco tissue cultures. Physiol Plant 15:473–497
15. Boudaoud A, Burian A, Borowska-Wykręt D, Uyttewaal M, Wrzalik R, Kwiatkowska D, Hamant O (2014) FibrilTool, an ImageJ plug-in to quantify fibrillar structures in raw microscopy images. Nat Protoc 9:457–463
16. Anderson CT, Carroll A, Akhmetova L, Somerville C (2010) Real-time imaging of cellulose reorientation during cell wall expansion in *Arabidopsis* roots. Plant Physiology 152:787–796
17. Jacques E, Verbelen J-P, Vissenberg K (2013) Mechanical stress in *Arabidopsis* leaves orients microtubules in a 'continuous' supracellular pattern. BMC Plant Biol 13:163
18. Parslow A, Cardona A, Bryson-Richardson RJ (2014) Sample drift correction following 4D confocal time-lapse imaging. J Vis Exp e51086
19. Xu T, Vavylonis D, Tsai F-C, Koenderink GH, Nie W, Yusuf E, I-Ju Lee, Wu J-Q, Huang X (2015) SOAX: A software for quantification of 3D biopolymer networks. Sci Rep 5:9081